Materials Research Express

PAPER • **OPEN ACCESS**

Low-temperature thermo-transport and magnetic properties of HfNiGe alloy

To cite this article: Md Mofasser Mallick and Satish Vitta 2025 *Mater. Res. Express* **12** 056303

Materials Research Express

PAPER

Low-temperature thermo-transport and magnetic properties of HfNiGe alloy

Md Mofasser Mallick[1] **and Satish Vitta**[2,3]

[1] Light Technology Institute, Karlsruhe Institute of Technology (KIT), 76131, Karlsruhe, Germany
[2] Department of Metallurgical Engineering and Materials Science, Indian Institute of Technology Bombay, Mumbai, 400076, India
[3] (Retired)

E-mail: mofasser.mallick@kit.edu

Keywords: intermetallic alloy, thermoelectric, magnetic, half-heusler

OPEN ACCESS

RECEIVED
18 February 2025

REVISED
12 April 2025

ACCEPTED FOR PUBLICATION
8 May 2025

PUBLISHED
21 May 2025

Abstract

XYZ-type intermetallic compounds exhibit a wide range of intriguing thermophysical properties. Here, we explore the low-temperature thermotransport behavior of a TiNiSi-type intermetallic alloy HfNiGe. The compound was synthesized using a high-temperature arc melting technique from high-purity elements, followed by annealing, pulverizing, and hot-pressing. The x-ray diffraction analysis reveals the presence of an orthorhombic phase belonging to space group pnma. The compound exhibits low electrical resistivity (ρ), increasing from 1 mΩ·cm to 2.5 mΩ·cm with temperature, characteristic of metallic behavior. The thermopower (α) values indicate an n-type system. It increases with temperature up to 150 K, reaching a maximum of $\sim -11\ \mu V{\cdot}K^{-1}$, before declining. The power factor (α^2/ρ) attains its highest value of $\sim 8\ \mu W{\cdot}m^{-1}{\cdot}K^{-2}$ at 186 K, while the maximum figure-of-merit (zT) of $\sim 5 \times 10^{-4}$ is observed at 207 K. Magnetic measurements suggest the presence of short-range ferromagnetic interactions with relatively high coercivity at room temperature. The temperature-dependent magnetic susceptibility (χ), measured under an external field of 50 Oe to 5 kOe, indicates Pauli paramagnetism along with the presence of paramagnetic impurities.

1. Introduction

XYZ-type intermetallic ternary alloys exhibit a wide diversity of physical and electronic properties, ranging from half-metallic ferromagnetic [1, 2], superconductivity [3, 4], and topological insulating [5–7] behavior to spintronics and thermoelectricity [8–11]. In the chemical formula XYZ, X represents the most electropositive and tipically transition metal or rare earth element, Z is the most electronegative and belongs to the main group element and Y is a transition metal [12, 13]. Many sub-groups belong to this type intermetallic alloys such as cubic half-Heusler phase (F4-3m) [14, 15], zincblende structure (F d -m 3) [16], ordered Fe_2P structure (P -6 2 m) [17] and TiNiSi type orthorhombic phase (pnma) [18]. Among them, the cubic half-Heusler phase with valence electron count (VEC) of 18 is a narrow band semiconductor with a band gap between ~0.1–0.5 eV. They also shows a high effective mass of charge carrier exhibiting high thermo-power [19–21]. Therefore, they have attracted significant attention for their good thermoelectric (TE) performance, often showing very high power factor values. However, while half-Heusler compounds exhibit a high power factor, they also show a high thermal conductivity which limits their resultant TE performance [22–24]. The TE efficiency of a material is defined by the dimensionless figure-of-merit $zT = S^2\sigma/k$, where S, σ, and κ are the Seebeck coefficient, electrical conductivity and the thermal conductivity respectively and $S^2\sigma$ is called power factor [25]. The thermal conductivity ($\kappa = \kappa_e + \kappa_L$), comprises of κ_e the electronic contribution and κ_L the lattice contributions. Therefore, to achieve a high zT, a TE material should have low thermal conductivity and a high power factor. Given that conventional half-Heusler alloys exhibit both high power factors and high thermal conductivities, this present study focuses on the HfNiGe alloy with a disordered atomic arrangement, which results in low

thermal conductivity [26]. In the TiNiSi-type orthorhombic structure of HfNiGe, all elements (Hf, Ni, or Ge) occupy 4c (x, $^{1}/_{4}$, z) positions with the same y (1/4) but different x and z without overlapping each other. Furthermore, it is found that multifunctional magnetic properties are also displayed by XYZ-type intermetallic alloy, especially by cubic half-Heusler phase. They transit between nonmagnetic to ferromagnetic behavior depending on the number of valence electron present in the compound. According to 'The Slater-Pauling rule', a half-Heusler alloy with valence electron count (VEC) $\boldsymbol{n_v}$ shows a magnetic moment (μ) = $\boldsymbol{n_v}$ −18 [27]. Hence half-Heusler compound with $\boldsymbol{n_v} > 18$ would show ferromagnetic behavior and with $\boldsymbol{n_v} = 18$ would show a nonmagnetic behavior. This present work investigates the magnetic and thermoelectric properties of TiNiSi-type orthorhombic HfNiGe with $\boldsymbol{n_v} = 18$. The study aims to comprehend the interplay between atomic disorder, thermal conductivity, and magnetism in the HfNiGe compound.

2. Experimental methods

2.1. Materials

Hafnium powder (Particle size 45 micron, purity 95.+%, Sigma-Aldrich), nickel powder (powder, <50 μm, 99.7% trace metals basis, Sigma-Aldrich), Germanium powder (chips, 99.999% trace metals basis, Sigma-Aldrich)

2.2. Preparation of the HfNiGe compound

TiNiSi-type orthorhombic compound HfNiGe was prepared using high-purity elements, Ti, Ni, and Ge by high-temperature arc melting in an Ar gas environment. First, the elements were weighed in a stoichiometric ratio to prepare a 5 g ingot. To avoid material loss during melting, the weighed elements were cold-pressed into a dense disc before arc melting. The solid disc was then placed in a water-cooled copper crucible and melted using an arc electrode. To achieve uniformity, the ingot of HfNiGe was flipped and melted multiple times. Further, to homogenize and remove the impurities present in the compound, the prepared ingot was annealed for 6 days at 1000 K in a vacuum-sealed quartz tube. The annealed ingot was pulverized into powder and consolidated into a disc using the hot-press technique under a pressure of 60 MPa for 2 h at 1273 K.

2.3. Characterization of the prepared HfNiGe compound

The consolidated disc was cut into a rectangular bar to measure the Seebeck coefficient (S), electrical resistivity (ρ), specific heat capacity (C_p), and thermal conductivity (κ) using a physical properties measurement system (PPMS) (Quantum Design) in the temperature range 2 K to 350 K. The remaining pieces of the annealed ingot were ground to make powder to study low-temperature magnetic properties in the temperature range 2 K to 300 K using a magnetic properties measurement system (MPMS), (Quantum Design SQUID magnetometer) in a magnetic field ranging from 0 to 20 kOe. The phase formation and crystallographic structure of the compound were analyzed by x-ray diffraction (XRD) technique on a PAN analytic x-ray analytical instrument with Cu Kα 1 radiation. Elemental and microstructural analyses were done by energy-dispersive x-ray Spectroscopy (EDS) and field emission scanning electron microscopy respectively. High-resolution micrograph and SAED pattern analysis were done using High-Resolution Transmission Electron Microscopy (HRTEM).

3. Results and discussion

3.1. Phase and microstructural analysis of the HfNiGe compound

Phase identification and crystallographic structural analysis were performed using x-ray diffraction technique. x-ray diffraction pattern along with Rietveld refinement of HfNiGe compund is shown in figure 1(a) [28]. It indicates that the compound is mostly a single-phase system with a small fraction of impurity phase. The XRD pattern of HfNiGe compound is found to be an orthorhombic TiNiSi type structure belonging to space group Pnma. The lattice parameters of the compound determined from Rietveld refinement are, $a = 6.41$ Å, $b = 3.81$ Å, and $c = 7.20$ Å respectively. The crystal structure and Fourier map along the [001] direction of the orthorhombic HfNiGe phase, are shown in figures 1(b) and (c).

A rectangular bar sample was used for chemical composition and microstructural analys using a scanning electron microscope. SEM image of polished surface and fracture surface of the HfNiGe compound are shown in figures 2(a)–(c) respectively. The SEM images indicates the formation of large grain. The EDS analysis was also performed to know the stoichiometric ratio of the elements in the compound. The result shows that the elements (Hf, Ni, Ge) present in the compound are almost equiatomic, it is found that Hf:Ni:Ge = 34.46:32.59:32.95 in at. %. High-resolution micrographs and SAED pattern of the compound is shown in figures 2(d)–(f). The TEM analysis indicates a polycrystalline system. The d-spacing of the lattice planes

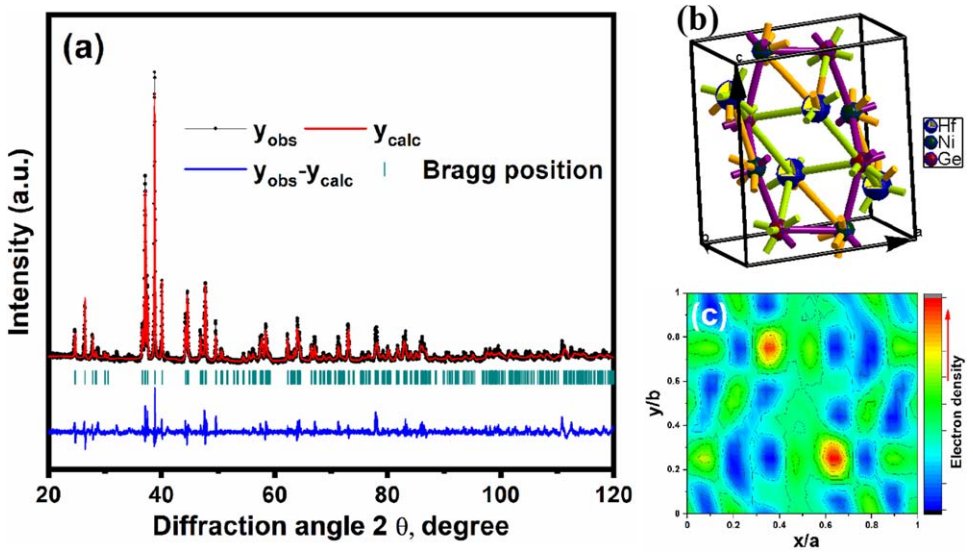

Figure 1. (a) Rietveld refinement results and XRD pattern for the orthorhombic HfNiGe phase at room temperature. (b) the crystal structure of the HfNiGe phase. (c) The Fourier map for electron density distributions of the atoms, Hf, Ni and Ge along [001] direction.

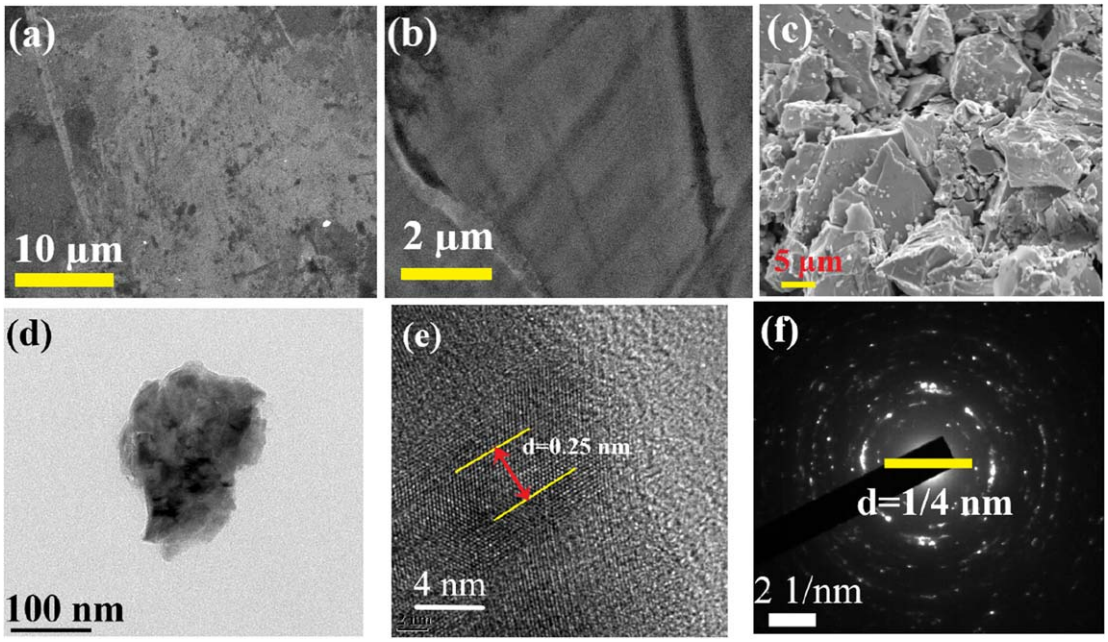

Figure 2. (a) & (b) SEM images of polished surface of the HfNiGe bar. (c) SEM image of fracture surface of the compound. (d) TEMimage, (e) HR-TEM micrograph and (f) SAED pattern of the compound HfNiGe.

calculated from the micrograph, which is found to be~0.25 nm. The estimated d-spacing is corresponding to the plane [210] which is also consistent with the XRD pattern.

3.2. Thermo-transport properties of the HfNiGe compound

Electrical transport parameters of the alloy have been determined using a Hall measurement system at room temperature. Carrier concentrations ($\boldsymbol{n_H}$), Hall mobility ($\boldsymbol{\mu_H}$), and the electrical resistivity (ρ) are found to be 1.81×10^{20} cm^{-3}, 14.2 cm^2 V^{-1}s^{-1}, and 2.43 mΩ-cm respectively. All low-temperature transport and thermoelectric properties of the compound are studied in the temperature range of 2 K to 350 K and the results are shown in figure 3. The specific heat capacity (C_p) increases with increasing temperature and reaches a maximum value of~0.23 Jg^{-1}K^{-1} and it becomes constant. The temperature-dependent C_p can be modeled using the equation; $C_p = \gamma T + \beta T^3$ where γ and β are the Sommerfeld coefficient corresponds to electronic

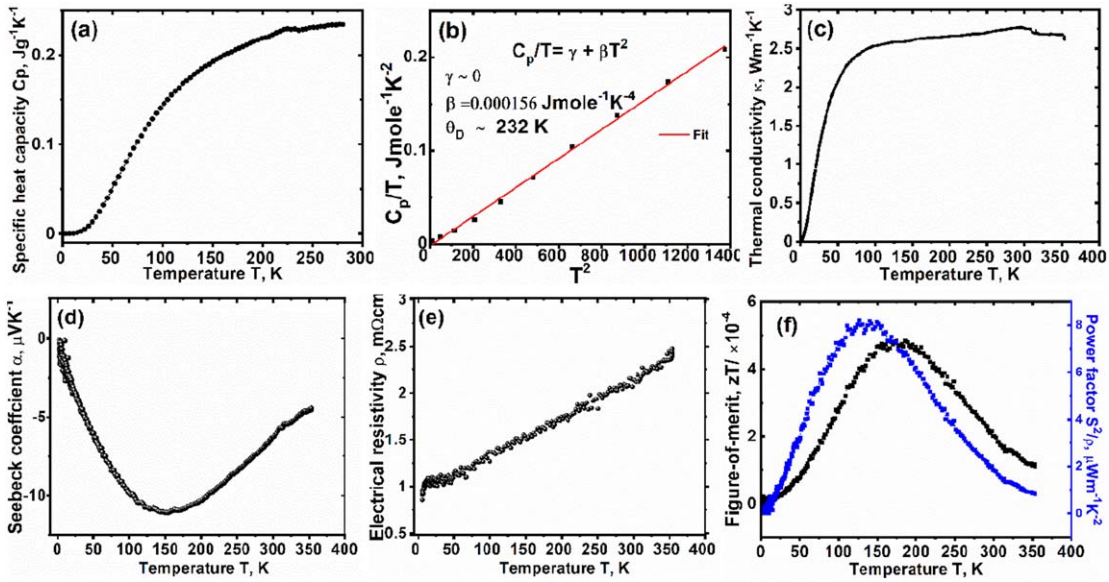

Figure 3. Temperature dependent (a) specific heat capacity C_p, (b) C_p /T and (c) thermal conductivity κ of the HfNiGe compound. The variation of (d) Seebeck coefficient α, (e) electrical resistivity ρ and (f) power factor and figure of merit of the HfNiGe alloy.

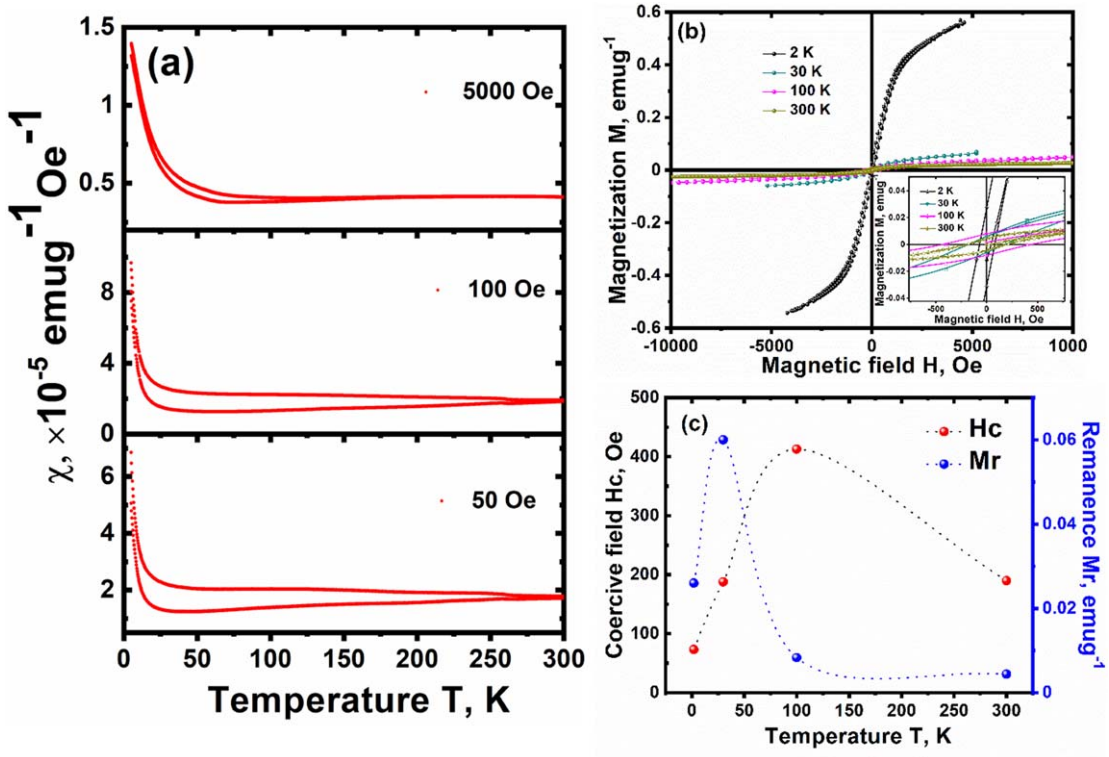

Figure 4. (a) The temperature dependent magnetic susceptibility χ of the HfNiGe compound for three different magnetic fields 50 Oe, 100 Oe and 5000 Oe. (b) Magnetic field dependent magnetization of the compound at 2 K, 30 K, 100 K and 300 K. (c) The variation of coercive field and remanence of the compound with temperature.

contribution and a coefficient corresponds to Debye-like phonon contribution respectively. The temperature coefficients γ and β are determined from the linearly fitting parameters of $\frac{C_p}{T} vs T^2$ plot at a low-temperature limit and it is found that $\gamma \sim 0$ and $\beta = 1.55 \times 10^{-4}$ Jmole^{-1}K^{-1} (cf figure 3(b)). The Debye temperature (θ_D) has been calculated via $\beta = 234\frac{k_B n}{\rho_m \theta_D^3}$, where n and ρ_m are the number density of atoms and the density of the compound respectively, and it is found that (θ_D) ~232 K. Rapid increase in thermal conductivity κ with

increasing temperature is found at T $<$ 100 K before reaching a maximum value of ~2.5 $Wm^{-1}K^{-1}$ beyond 100 K and then it remains constant even at room temperature (cf figure 3(c)). The κ is a considerably very low value for XYZ type intermetallic alloys like half-Heusler alloys.

The thermopower (α) of the compound is negative in the complete temperature range indicating an n-type system and it increases with increasing temperature till 150 K, after reaching a maximum value of ~-11 μVK^{-1} starts decreasing with temperature which is probably due to bipolar conduction (cf figure 3(d)). The electrical resistivity(ρ) increases with increasing temperature in the complete temperature range, a metallic behavior, and the absolute value of ρ is low and varies from~1 mΩ-cm to 2.5 mΩ-cm which is consistent with Hall measurement data (cf figure 3(e)). However, a change in slope, sharp decreasing trend, of electrical resistivity is found at ~5 K, and at the same temperature there is a sharp peak in the temperature-dependent thermopower (α) plot probably indicating a structural transition. The power factor (α^2/ρ) has been calculated from α and ρ, with increasing temperature it also increases and reaches the highest value of ~8 $\mu Wm^{-1}K^{-2}$ at 186 K before decreasing at a higher temperature. A maximum figure-of-merit (zT) value of ~5×10^{-4} is found at 207 K.

3.3. Magnetic properties of the HfNiGe compound

To investigate the magnetic behavior of the compound, both the temperature T and external magnetic field H-dependent magnetization, M has been studied in the temperature range 2 K to 300 K. The temperature dependence magnetic susceptibility χ of the alloy in the presence of 50 Oe to 5 kOe external field under both zero-field cooled (ZFC) and field cooled (FC) states is shown in figure 4(a). Irreversibility in magnetization under ZFC and FC states is detected at all fields in the χ-T plot, probably because of the existence of magnetically ordered states and it is observed that at 5 kOe this irreversibility is reduced indicating elimination of magnetically order phases present in the system at high field. However, there is no significant change in magnetic susceptibility χ is found at temperature T $>$ 30 K indicating a Pauli paramagnetic compound. The increment of χ at T $<$ 30 K is due to probably paramagnetic impurities present in the compound which are undetected by the x-ray diffraction pattern. The variation of magnetization with the magnetic field of the compound in the range $\pm$10 kOe at different temperatures is shown in figure 4(b). The interesting features which are observed from field-dependent magnetization studies are–(i) M decreases with increasing T which is consistent with χ-T plot (ii) high coercivity Hc is found at all temperatures varying from 12 Oe to 413 Oe and the highest coercivity of the alloy is found at 100 K, shown in figure 4(c) (iii) the remanence Mr of the alloy is low and maximum Mr of~0.06 $emug^{-1}$ is achieved at 30 K. However, various type of magnetic behavior observed from experimental studies indicates that unlike conventional XYZ-type cubic half-Heusler alloy belonging to the space group F 4-3m, the HfNiGe alloy shows unusual magnetic features like ferromagnetic interaction at room temperature. According to the Slater-Pauling rule, the magnetic moment μ of a cubic half-Heusler intermetallic alloy with valence electron count (VEC) n_V can be expressed as $\mu = n_V - 18$ and the alloy with $n_V = 18$ should be nonmagnetic behavior. In this case, even though the alloy is not a half-Heusler phase, HfNiGe with $n_V = 18$ exhibits different magnetic indications.

3.4. Discussion

From the characterizations, two notable findings in the HfNiGe compounds are the low thermal conductivity and the presence of ferromagnetic interactions. Despite its high electrical conductivity, the low thermal conductivity in HfNiGe is a distinguished characteristic of system. Previous reports suggest that the thermal transport properties of TiNiSi-type orthorhombic phases are primarily governed by their intrinsic lattice structures. Especially, the presence of a chair-shaped ⋯Si–Ni–Si–Ni⋯ framework—analogous to that observed in ultralow thermal conductivity SnSe, where coherent phonon propagation is disrupted strongly [29, 30]. In HfNiGe, this feature, along with edge-sharing polyhedral connectivity and anisotropic bonding environments facilitates strong phonon scattering, leading to inherently low lattice thermal conductivity. Furthermore, the coupling between magnetic ordering and lattice vibration could also enhance phonon scattering via spin-phonon interactions. Although this phenomena has not been investigated for HfNiGe compound, previous reports indicate how magnetic fluctuations and domain structures can impact thermal conductivity [31, 32]. As the ferromagnetic interactions and atomic disorder found, these factors may jointly contribute to the low thermal conductivity in HfNiGe compound. As result, the thermal conductivity of the HfNiGe compound is found be significantly lower compared to other XYZ type alloys [19]. A more detailed experimental and computational studies on this phenomena would facilitate a valuable insight.

4. Conclusion

TiNiSi type ternary intermetallic alloy HfNiGe has been synthesized, and its low-temperature thermotrasport properties have been thoroughly investigated. Several interesting transport phenomena have been identified.

Particularly, two notable findings are (a) an inherently low thermal conductivity, and (b) the presence of ferromagnetic interactions. Although thermopower, as well as the power factor of the alloy, is not yet sufficiently high for thermoelectric application, the thermal conductivity of the alloy is found to be very low even at room temperature, ~2.5 $Wm^{-1}K^{-1}$ which is substantially lower than that of conventional cubic half-Heusler phases. This result suggests that with further optimization of charge transport, the Seebeck coefficient could potentially be enhanced, leading to higher performance. Furthermore, Unlike conventional cubic half-Heusler alloys, HfNiGe with valence electron count ($n_V = 18$) exhibits different types of unusual magnetic features such as ferromagnetic interaction with high coercivity. This opens up a new aspect of the HfNiGe based compound for magnetic applications.

Acknowledgments

The authors wish to acknowledge Nano mission, Govt. of India and Space Technology Cell-IIT Bombay for financial assistance and the Indian Institute of Technology Bombay for provision of various characterization facilities. The authors acknowledge funding by the European Research Council, grant 101097876—ORTHOGONAL.

Data availability statement

The data cannot be made publicly available upon publication because no suitable repository exists for hosting data in this field of study. The data that support the findings of this study are available upon reasonable request from the authors.

ORCID iDs

Md Mofasser Mallick https://orcid.org/0000-0003-2105-6153
Satish Vitta https://orcid.org/0000-0003-4138-0022

References

[1] Manandhar B, Dahal P S, Nepal S and Baral A 2022 Electronic and magnetic properties of half heusler alloy NiCrSi *Himal. J. Sci. Technol.* **6** 96–9
[2] Abada A and Marbouh N 2020 Study of new d0 half-metallic half-heusler alloy MgCaB: first-principles calculations *J. Supercond. Nov. Magn.* **33** 889–99
[3] Kim J, Fijalkowski K M, Kleinlein J, Schumacher C, Markou A, Gould C, Schreyeck S, Felser C and Molenkamp L W 2023 Molecular beam epitaxy of a half-Heusler topological superconductor candidate YPtBi *Phys. Rev. Mater.* **7** 024802
[4] Messaoudi C, Mir A, Mekhazni Y and Cherchab Y 2022 Discovery of the kagome superconductor in the half-heusler 'NbRhSb *Eur. Phys. J. Plus* **137** 1089
[5] Singh A K, Ramarao S D and Peter S C 2020 Rare-earth based half-Heusler topological quantum materials: a perspective *APL Mater.* **8** 060903
[6] Shirokura T, Fan T, Khang N H D, Kondo T and Hai P N 2022 Efficient spin current source using a half-Heusler alloy topological semimetal with back end of line compatibility *Sci. Rep.* **12** 2426
[7] Shirokura T, Kondo T and Hai P N 2022 Effect of stoichiometry on the spin hall angle of the half-heusler alloy topological semimetal YPtBi *Jpn. J. Appl. Phys.* **61** 073001
[8] Casper F, Graf T, Chadov S, Balke B and Felser C 2012 Half-heusler compounds: novel materials for energy and spintronic applications *Semicond. Sci. Technol.* **27** 063001
[9] Rogl G and Rogl P F 2023 Development of thermoelectric half-heusler alloys over the past 25 years *Crystals* **13** 1152
[10] Elphick K, Frost W, Samiepour M, Kubota T, Takanashi K, Sukegawa H, Mitani S and Hirohata A 2021 Heusler alloys for spintronic devices: review on recent development and future perspectives *Sci. Technol. Adv. Mater.* **22** 235–71
[11] Xiao H, Hu T, Liu W, Zhu Y L, Li P G, Mu G, Su J, Li K and Mao Z Q 2018 Superconductivity in the half-Heusler compound TbPdBi *Phys. Rev.* B **97** 224511
[12] Graf T, Felser C and Parkin S S P 2011 Simple rules for the understanding of Heusler compounds *Prog. Solid State Chem.* **39** 1–50
[13] Mallick M M and Vitta S 2017 Thermophysical and magnetic properties of p- and n-type Ti-Ni-Sn based half-heusler alloys *J. Alloys Compd.* **710** 191–8
[14] Vishali D and John R 2022 Structural, electronic and magnetic properties of the Half-Heusler alloy CrZSi (Z = Sc, Ti) *J. Cryst. Growth* **583** 126556
[15] Xia K, Hu C, Fu C, Zhao X and Zhu T 2021 Half-heusler thermoelectric materials *Appl. Phys. Lett.* **118** 140503
[16] Dessenne F, Cichocka D, Desplanques P and Fauquembergue R 1997 Comparison of wurtzite and zinc blende III-V nitrides field effect transistors: a 2D Monte Carlo device simulation *Mater. Sci. Eng.* B **50** 315–8
[17] Swainson I P, Wu W, McCollam A and Julian S R 2010 Non-collinear antiferromagnetism in FeCrAs special issue on neutron scattering in Canada *Can. J. Phys.* **88** 701–6
[18] Zhang T, Gong Y, Wang B, Cen D and Xu F 2022 Crystallography of the martensitic transformation between Ni2In-type hexagonal and TiNiSi-type orthorhombic phases *J. Mater. Sci. Technol.* **104** 59–66
[19] Quinn R J and Bos J W G 2021 Advances in half-heusler alloys for thermoelectric power generation *Mater. Adv.* **2** 6246–66

[20] Mallick M M and Vitta S 2018 Enhancing the thermoelectric performance of a p-type half-Heusler alloy, HfCoSb by incorporation of a band-matched chalcogenide, Cu_2Te *J. Mater. Chem.* A **6** 14709–16
[21] Mallick M M, Rajput K and Vitta S 2019 Increasing figure-of-merit of ZrNiSn half-heusler alloy by minimal substitution and thermal conductivity reduction *J. Mater. Sci., Mater. Electron.* **30** 6139–47
[22] Bahrami A, Ying P, Wolff U, Rodríguez N P, Schierning G, Nielsch K and He R 2021 Reduced lattice thermal conductivity for half-heusler ZrNiSn through cryogenic mechanical alloying *ACS Appl. Mater. Interfaces* **13** 38561–8
[23] Kennedy B F, Kimber S A J, Checchia S, Shawon A K M A, Zevalkink A, Suard E, Buckman J and Bos J W G 2023 Thermoelectric properties of the aliovalent half-Heusler alloy Zn0.5Ti0.5NiSb with intrinsic low thermal conductivity *J. Mater. Chem.* A **11** 23566–75
[24] Tranås R, Løvvik O M and Berland K 2022 Attaining low lattice thermal conductivity in half-heusler sublattice solid solutions: which substitution site is most effective? *Electron. Mater.* **3** 1–14
[25] Terasaki I 2011 Introduction to thermoelectricity *Materials for Energy Conversion Devices* 339–57
[26] Mallick M M and Vitta S 2016 Thermoelectric properties of ultra-low thermal conductivity half-Heusler alloy *AIP Conf. Proc.* **1731** 110027
[27] Galanakis I 2016 Theory of heusler and full-heusler compounds *Springer Ser. Mater. Sci.* **222** 3–36
[28] Sakata M and Cooper M J 1979 An analysis of the rietveld refinement method *J. Appl. Crystallogr.* **12** 554–63
[29] Saurabh K, Kumar A, Ghosh P and Singh S 2021 Low thermal conductivity and semimetallic behavior in some TiNiSi structure-type compounds *Phys. Rev. Mater.* **5** 085406
[30] Zhao L D, Lo S H, Zhang Y, Sun H, Tan G, Uher C, Wolverton C, Dravid V P and Kanatzidis M G 2014 Ultralow thermal conductivity and high thermoelectric figure of merit in SnSe crystals *Nature* **508** 373–7
[31] Dixon G S 1980 Lattice thermal conductivity of antiferromagnetic insulators *Phys. Rev.* B **21** 2851–64
[32] Jena A, Lee S C and Bhattacharjee S 2021 Tuning the lattice thermal conductivity in bismuth telluride via Cr alloying *Phys. Rev. Appl.* **15** 064023